ACS APPLIED MATERIALS & INTERFACES

Research Article

www.acsami.org

Hydrolytic Stability of Mesoporous Zirconium Titanate Frameworks Containing Coordinating Organic Functionalities

Massey de los Reyes,[†,‡] Peter J. Majewski,[‡] Nicholas Scales,[†] and Vittorio Luca*[,§]

[†]Institute of Materials Engineering, Australian Nuclear Science and Technology Organisation, Locked Bag 2001, Kirrawee DC, New South Wales, 2232, Australia

[‡]School of Advanced Manufacturing and Mechanical Engineering, Mawson Institute, University of South Australia, Mawson Lakes Blvd, Mawson Lakes, SA 5095, Australia

[§]Centro Atómico Constituyentes, Comisión Nacional de Energía Atómica, Avenida General Paz 1499, 1650 San Martín, Provincia de Buenos Aires, Argentina

Supporting Information

ABSTRACT: The hydrolytic stability of lanthanide and actinide selective mono- and polyphosphonate-functionalized mesoporous zirconium titanium oxide adsorbents has been investigated in nitric acid solutions. Hydrolytic degradation of the surfaces, as measured through the fractional loss of phosphorus and elements of the oxide framework, increased by more than an order of magnitude as the nitric acid concentration was increased from 0 to 2 mol/L. The unfunctionalized parent oxide suffered considerable dissolution in 2 mol/L acid over a period of 72 h. Under identical conditions, the fractional Zr and Ti release was reduced to 1×10^{-2} for monophosphonate functionalized hybrids and reached as low as 1×10^{-6} for trisphosphonate functionalized variants. The bisphosphonates showed intermediate values. The leaching of P, Zr and Ti was found to be incongruent with the Zr leaching to a lesser extent implying enhanced stability of the Zr−O−P bond. Quantitative analysis of the dissolution kinetics indicated a parabolic dissolution model with a rate constant in the range of 0.5−1.5 mg g^{-1} $min^{-1/2}$ for the elemental leaching of P, Ti, and Zr. The leaching of Zr from the mesoporous matrix was relatively more complex than for the other elements with evidence of a leaching mechanism involving two processes. ToF-SIMS and DRIFT analysis demonstrated that after leaching in 2 M HNO_3 for 24 h, a significant proportion of grafted ligands remained on the surface. The oxide functionalized with amino trismethylenephosphonic acid, which had previously shown excellent $^{153}Gd^{3+}$ selectivity, was demonstrated to have outstanding stability, with low fractional elemental losses and preservation of mesoporous texture even after leaching for 24 h in 2 M HNO_3. This suggests this particular hybrid to be worthy of additional study.

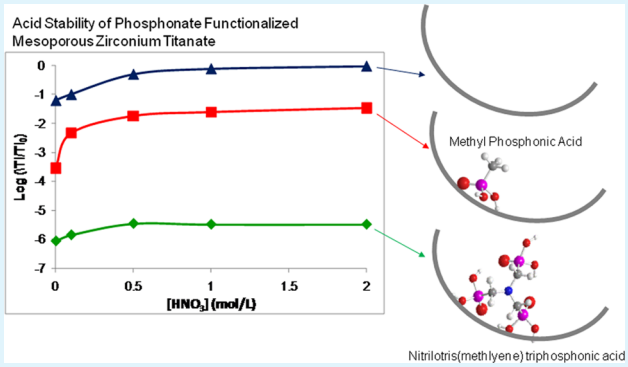

KEYWORDS: *mesoporous, zirconium, titanium, phosphonic acid, phosphonate, functionalization, hydrolytic stability, leaching*

1. INTRODUCTION

Functionalized mesoporous adsorbents (FMA) comprising a mesoporous metal oxide framework to which is grafted a multifunctional organic molecule with one or more grafting and binding groups represent an interesting class of solid phase extractant materials, the development of which has attracted an extraordinary amount of interest in the past decade.[1] Being hydrid materials, FMA systems offer properties that are intermediate between those of purely inorganic adsorbents and organic polymer resin systems. FMA materials can have extremely high surface areas and offer immense scope for tailoring properties primarily through the choice of framework composition and functional groups to suit particular adsorption applications.

The context of the present contribution is the development and application of FMA materials for the removal of radioactivity from the environment, reactor cooling circuits, the pretreatment of radioactive wastes resulting from radioisotope production and the reprocessing of spent fuel. The isotopes of most concern are typically fission products with long half-lives and high radiotoxicities including the likes of ^{137}Cs, ^{90}Sr, and ^{129}I, along with actinides and minor actinides such as ^{241}Am. Fryxell and co-workers were among the first to address the use of organically functionalized mesoporous silicate adsorbents for the separation of radioactive elements.[2] Those materials were based on functionalization with silane terminated glycinyl-urea, salicylamide and acetamide phosphonate molecules. The latter materials showed good selectivity for

Received: December 28, 2012
Accepted: April 12, 2013
Published: April 12, 2013

the major actinides, U, Th, and Pu at pH values less than two but relatively poor selectivity for minor actinides at these pH values. The use of FMAs for the adsorption of major actinides such as uranium and thorium has also been considered very recently.[3,4]

An important advantage of FMA systems that became apparent to us was the fact that once they become saturated with the target radionuclides, simple avenues to disposition were available.[5] One option for instance is direct calcination of the saturated adsorbent to produce a product from which the radioactive elements can not escape into the environment. Althouh saturated functionalized mesoporous silicates can lead to nuclear glasses, other compositions can lead to ceramics or glass-ceramics, which are potentially even more stable.

With the above in mind, in about 2004, we embarked on the preparation of mesoporous zirconium titanium mixed oxide xerogels.[5] It was shown that saturation of this mesoporous material with calcium led to zirconolite at lower temperatures than achievable through conventional oxide processing. Zirconolite is an important ceramic material in a radioactive waste management context because actinides can be incorporated into the structure and are rendered highly resistant to leaching.[6−8] It was later also demonstrated that the mesoporous zirconium titanium oxide xerogels possessed interesting and useful adsorption properties.[9] However, improved selectivity of the mixed oxide required surface functionalization with suitable organic molecules. Although many studies had previously been published on the grafting of monophosphonates to titania nanoparticles[10−13] and mesoporous titanates,[14] relatively little work has been undertaken on the grafting of polyphosphonates to mesoporous mixed metal oxides. Polyphosphonates offer the potential for enhanced stability through strong binding to the mixed oxide framework as highlighted very recently.[15] Thus, excellent selectivity for the adsorption of lanthanides and actinides was demonstrated for mesoporous zirconium titanium oxide xerogels the surfaces of which had been functionalized with bis- and trisphosphonates.[16] The next step in the development of this new FMA system was to engineer materials in a form suitable for use in fixed bed column applications. Fully inorganic mesoporous zirconium titanium mixed oxides beads were thus prepared and were shown to have limitations in terms of their kinetics.[17] This then led to the preparation of amino trimethylene trisphosphonate-functionalized (ATMP) hierarchical bead materials displaying excellent selectivity and rapid kinetics through a dual templating strategy.[17]

The functionalized mesoporous zirconium titanium oxides developed to date have been demonstrated to have considerable potential for the adsorption of nonradioactive heavy metals such as lanthanides. Indeed, Makowski and coworkers[18] have recently highlighted the potential usefulness of such materials in nuclear applications. In such applications, it is paramount that the materials be able to operate for extended periods without suffering significant degradation of adsorption properties. As the adsorbents concentrate target radioactive species, they become increasingly subject to radiolytic degradation. Apart from radiolytic damage of the FMA materials, hydrolysis of the link between the inorganic framework and the functional molecule and the loss of functionality is also a potential weakness of these systems. Most typically, this link is an M−O−Si or M−O−P bond when silanes and phosphonates are used for grafting. Although mesoporous silicates to which have been grafted amino chlorosilanes and alkoxysilanes appear relatively stable in water at near neutral pH values,[19] at pH values far from neutral, the stability has been shown to be limited.[20]

The importance of hydrolytic and radiolytic stability can not therefore be overstated if further development and application of novel phosphonate-functionalized mesoporous mixed metal oxides in demanding applications is to be realized. The need to quantitatively measure the hydrolytic and radiolytic stability and come to an understanding of the degradation mechanisms is therefore necessary and forms the aim of the present work. Mesoporous zirconium titanium oxide xerogels were prepared by previously established methods and functionalized with a range of different organophosphonate coupling agents containing from one to three phosphonate groups in a manner similar to that previously described.[16] These hybrid materials were subjected to different leaching regimes that included measuring the kinetics of dissolution in acids of different concentration. The leached materials were subsequently thoroughly characterized in an attempt to better understanding the processes involved.

2. EXPERIMENTAL SECTION

2.1. General. All materials, reagents and solvents were of AR grade (Sigma-Aldrich, Fluka) and were used without further purification. Methylphosphonic acid (MeP), phenylphosphonic acid (PPA), 1-hydroxyethane 1,1-diphosphonic acid or etidronic acid (HEDP), N-(phosphonomethyl) iminodiacetic acid (PIDC), and 4-amino,1-hydroxy,1,1-*bis*-phosphonic acid or alendronate (HABDP) were sourced from Aldrich and were used as received along with amino trimethlyenetriphosphonic acid (ATMP) that was obtained as a 50 wt % aqueous solution and was also used as received.

2.2. Synthesis of Zirconium Titanium Oxide Mesoporous Xerogels. Mesoporous zirconium titanium oxides (mZrTi) affording a (Zr/(Zr + Ti) ratio of 0.33 were prepared using a previously employed methodology.[5] Briefly, in a nitrogen filled glovebox, the required stoichiometric ratios of zirconium propoxide (70% w/w in propanol) and titanium isopropoxide (97%) were combined along with an in-expensive long-chain palmitic acid surfactant (C_{18}) acting as a porogen, accounting for a metal:surfactant ratio of 2. Gentle heating of the mixtures allowed the solid carboxylate to dissolve at approximately 70 °C. This was followed by incubation in a closed chamber with typically 70 - 80% relative humidity passed over the precursor solutions at a constant temperature of 30 °C. An air flow of approximately 300 mL/min was used for the volatilization of the alcohols and partial hydrolysis to initiate formation of the mesoporous metal oxide structure. The colloidal gels were aged until they became viscous before being poured into deionized water to complete the hydrolysis and condensation reactions. Finally, the solids obtained were filtered, dried at 80 °C, and finally calcined overnight at 450 °C for 7 h to generate a porous network.

2.3. Functionalization of Zirconium Titanium Oxide Mesoporous Xerogels. Surface functionalization with different phosphonate and polyphosphonate molecules was carried out following a previously described procedure with some minor variations.[16] Briefly, 4 g of as-prepared mZrTi material was ground gently and contacted with an appropriate phosphonic acid solution (41 mM) for 24 h with shaking at 130 rpm in a tightly sealed glass bottle. The pH of the mixture was not adjusted. The solid was then filtered using a Buchner funnel and washed several times with deionized water until the solution pH was neutral. After drying at 80 °C for 24 h, it was then transferred into a vacuum oven (10 mmHg, 50 °C) for a further 10 h. The phosphonic acid functionalized mesoporous phases will be referred to by P-mZrTi.

2.4. Leaching Procedure. Batch leaching experiments were carried out under varying nitric acid concentrations (0.001−2 M) at room temperature (24−25 °C) in an open atmosphere. Investigations in the alkaline region showed significant degradation of the matrix,

consistent with previous results obtained with works of others; hence no further tests were carried out.[21] Approximately 150 mg of either functionalized or parent material (mZrTi) was weighed into a 20 mL high density polyethylene vial with 15 mL of a given HNO_3 concentration and contacted for periods of 24 or 72 h on an orbital shaker and agitated at 140 rpm. All samples were examined in duplicate and standards were included as a check on the reliability of the data using a mass to volume ratio (V/m) of 100 mL/g. Once the duration of the tests was complete, samples were filtered using 0.45 μm syringe filters with the leachate collected in clean polyethylene vials. Samples were then analyzed for elemental release (P, Ti, and Zr) using ICP-MS (Perkin-Elmer Elan 6000). The fractional release f was normalized in terms of the materials surface area. For all P, Ti, and Zr leached into solution, f was calculated as follows

$$f = \frac{(W_0 - W_t)}{W_t} \quad (1)$$

Here, W_0 is the initial elemental content in the solid phase and W_t is the elemental content remaining in the solid phase after time t. The amount of Zr and Ti in the mixed mesoporous material is based on the compositional ratio $(Ti_{0.33}, Zr_{0.66})O_2$. Results are given in log form to emphasize in f for the various elements in different materials. The pH before and after leaching was measured using a combined glass electrode standardized with buffers of pH 4, 7, and 9. The change in solution pH during experiments and after equilibration time was only ±0.1 units.

2.5. Statistical Analysis. To determine the significance of P, Ti and Zr release kinetics of individual time points over 24 h, a one-way analysis of variance (ANOVA) was determined. From this analysis, the key factor is the Poisson-regression (p) value, which is generically set at $p = 0.05$ (5%); for statistical significance, a p value must be lower than this to be deemed significant.

2.6. Characterization. Thermogravimetric analyses (TGA) and differential thermal analyses (DTA) were conducted simultaneously on a Setaram TAG24 (France) with high purity instrument air as the carrier gas. Before analysis, the parent and functionalized mesoporous phases were dried (50 °C, 10 mmHg, 12−14 h) to remove most of the physisorbed water so as to enable an accurate determination of the temperature at which the functionalized organic molecule was thermalized from the mesoporous phase. Calculation of the degree of functionalization has been expressed as the number of organic molecules per nm^2. Specific surface areas of the materials were determined using nitrogen gas adsorption on a Micromeritics ASAP 2010 instrument using the BET method.

Diffuse reflectance FT-IR (DRIFT) of the dried parent and functionalized mesoporous phases were recorded in KBr (5% w/w) in the range 4000−650 cm^{-1} with a Nicolet Nexus 8700 FT-IR spectrometer equipped with a liquid nitrogen-cooled HgCdTe detector and a Thermo Electron diffuse reflectance (DRIFT) accessory.

Phosphorus-31 solid-state magic angle spinning (MAS) nuclear magnetic resonance (NMR) data were acquired at ambient temperature on a Bruker MSL-400 spectrometer operating at a ^{31}P frequency of 161.92 MHz. Conventional single-pulse (Bloch decay) experiments with high-power ^1H decoupling during acquisition and cross-polarization experiments were implemented on a Bruker 4 mm double-air-bearing probe utilizing MAS frequencies of 0 kHz. The single-pulse experiments used $\pi/4$ excitation pulses with recycle delays of 20s. All ^{31}P chemical shifts were measured with respect to 85% H_3PO_4 via an external sample of $(NH_4)H_2(PO_4)$, which was also used to establish the Hartmann−Hahn match condition.

ToF-SIMS spectra were acquired using a Physical Electronics PHI model TRIFT II spectrometer, with a high mass resolution of 9000 and a high transmission greater than 50%. Sample surfaces were calibrated at 3 kV with respect to the grounded extraction electrode for positive and negative mode SIMS respectively. The gallium (Ga^+) liquid metal primary ion source was operated with varying currents of 20, 60, and 600 pA, a pulse length of 15−60 ns and a separation rate of 11 kHz. The analyzed area was approximately 84 × 84 μm^2 and the total ion dose used to acquire each spectrum approximately 10^2 ions/cm^3 ensuring static SIMS conditions. Resulting data was analyzed using the WinCadence software suite.

Nitrogen adsorption−desorption isotherms were recorded at 77 K on a Micromeritics ASAP2020 instrument. Specific areas were calculated using the BET method while pore size distributions (PSD) were determined using BJH as well as nonlocalized density functional theory.

3. RESULTS AND DISCUSSION

3.1. Sample Characterization. TGA-DTA analyses were undertaken to determine the level of surface functionalization by evaluating the percentage mass loss of the grafted molecules between 200 and 600 °C following previously defined procedures.[16] Accordingly, the samples were dried in an 80 °C oven followed by further drying under vacuum (10 mmHg, 50 °C) to remove residual physi-sorbed water, preventing mass losses less than 1.5% w/w at temperatures below 200 °C. The degree of surface loading is summarized in Table 1, where

Table 1. Phosphonic Acid Functionalization onto mZrTi (P/nm^2/g)

sample description[a]	temp range (°C)	2nd stage mass loss (%)	P (nm^2/g (calcd))[b]
Me-P-mZrTi	200−600	4.1	6.2
PPA-mZrTi	200−500	5.5	0.94
HEDP-mZrTi	200−485	3.7	1.9
PIDC-mZrTi	200−480	5.9	0.92
HABDP-mZrTi	200−550	3.8	0.97
ATMP-mZrTi	200−500	3.0	1.2

[a]Me-P = methylphosphonic acid; PPA phenylphosphonic acid; HEDP = 1,1-diphosphonic acid; PIDC = N-(phosphonomethyl) iminodiacetic acid; HABDP = 4-amino, 1-hyroxy, 1,1-*bis*-phosphonic acid; ATMP = amino trismethlyenephosphonic acid. [b]Functionalization normalized with a surface area of 264 m^2/g.

functionalization has been normalized relative to the surface area of the mesoporous material (m^2/g). For the purpose of illustration, representative TGA/DTA curves can be found in the Supporting Information section (Figure S1). In line with our previous results for similar samples, the polyphosphonate functionalized variants showed loadings in the range 0.9 to 6 P/nm^2/g (Table 1) demonstrating that the sample-to-sample variations are acceptable despite slight variations in the preparation procedures between the present and earlier work. The significantly higher loading obtained for the monophosphonate-functionalized material (MeP-mZrTi) could be due to greater sensitivity of monophosphonate grafting to small variations in the surface area of the parent mZrTi and reduced stearic effects. These loading results suggest that functionalization occurs by distinctly different mechanisms, influenced by the potential mode of coordination to the surface. Although differences may also arise from chain entanglement, it has been shown that phosphonic acids containing chains that lie flat or oriented with large tilt angles relative to the surface can produce lower degrees of monolayer formation and chain ordering through steric blocking of substrate binding sites.[22]

Detailed spectroscopic characterization of the phosphonate functionalized materials was performed by DRIFT and ^{31}P MAS NMR spectroscopies as per our previous study and the results for the present samples were broadly consistent with those previously reported (see Table S2 in the Supporting Information section).[16]

3.2. Effect of Acid Concentration on Leaching.

3.2.1. Phosphorus Release. To determine the influence of increasing nitric acid concentration on the hydrolytic stability of the hybrid materials, leaching experiments were performed using HNO_3 concentrations in the range 0.001−2 mol/L under ambient temperatures for 24 and 72 h (Figure 1). For the MeP

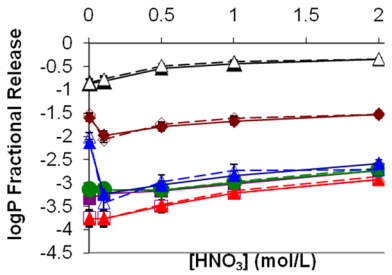

Figure 1. Leaching of P from P-mZrTi materials in varying HNO_3 concentrations (2−0.001 mol/L) for 24 and 72 h; Me-P (black filled and open triangles), PPA (brown filled and open diamond), HEDP (blue filled and open triangle), PIDC (green filled and open circle), HABDP (purple filled and open square) and ATMP (red filled and open triangle). (Note that the uncertainties (error bars) at some data points are smaller than the symbol).

functionalized mZrTi a smooth increase in the phosphorus leached fraction is observed for HNO_3 concentrations of 0.001 to 2 mol/L. The next most easily leached hybrid material was the PPA-mZrTi phase. In this case from the lowest HNO_3 concentration of 0.001−0.1 mol/L there was a measurable initial drop in the fraction of P leached whereas from 0.1 to 2 mol/L of HNO_3 the leached fraction also increased smoothly. A similar reduction in initial leached fraction was also observed for HEDP but not for the other materials. This initial drop could be due to a decrease in concentration, with most of the protons acidifying the surface to produce M−OH rather than hydrolyzing M-O-P bonds. The data of Figure 1 show that by far the greatest degree of phosphorus leaching occurred for MeP-mZrTi. The only other monophosphonate investigated with no other (nonphosphonate) potential binding groups, PPA, was also relatively easily leached. In comparison to the monophosphonates, the fraction of P leached from the polyphosphonate functionalized materials was significantly lower. Although the PIDC molecule also contains a single phosphonate group, it also contains two carboxylate groups that can potentially bind to titanate surfaces as has been demonstrated in the past.[23] Thus, the ostensibly high leach resistance of this hybrid can be rationalized on the basis of binding by multiple anchor groups. In each case, only trace amounts of P (~100 ppm) were detected in solution by ICP-MS. The binding strength of each ligand under increasing acidic conditions for the investigated time periods increases in the following order; ATMP > HABDP ≈ PIDC > HEDP > PIDC > PPA > Me-P. It must be noted that this work is the first to quantify the acid leachability and the potential surface stability of both phosphonate and polyphosphonate molecules on the mesoporous surfaces of zirconium and titanium mixed oxide. Other investigations have focused only on monophosphonates but not bis- and tris-phosphonate hybrids.[24−26] The advantage of polyphosphonates relative to monophosphonates is clearly evident since the latter ligands leach out to a far greater extent than the former. Like PIDC, HABDP also possesses an alternative potential anchor group (the amine), that is known to covalently anchor to oxide surfaces successfully through direct assembly.[27] Although PIDC offers potential for coordination of the carboxylate groups its stability is reduced compared with HEDP, HABDP and ATMP. Indeed the literature suggests that a P−O−M coordination is more stable toward hydrolysis than a C−O−M linkage.[28] The greater strength and stability of the phosphoryl P═O bond dominates a substantial part of phosphorus chemistry, however, dissolution is seen when the oxygen atom is involved in a bridge as in P−O−P or P−O−C linkages, which generally results in hydrolytic instability and the material is therefore prone to nucleophilic attack by H^+ ions when acidity increases, cleaving them into solution.[29,30] Moreover, the amount of ligand on the surface is independent to the amount leached in solution according to TGA-DTA analysis, with similar surface functionalizations produced for each PIDC, PPA, ATMP and HABDP at 1 P/(nm^2 g), but collectively generating different leached fractions. Differences in ligand size may also contribute to leaching behavior.

3.2.2. Titanium Leaching. Fractional titanium release from P-mZrTi and unfunctionalized mZrTi materials as a function of acid concentration are displayed in Figure 2. It is evident that

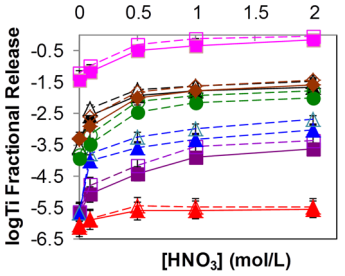

Figure 2. Leaching of Ti from mZrTi and P-mZrTi materials in varying HNO_3 concentrations (2−0.001 mol/L) for 24 and 72 h; mZrTi (pink filled and open squares), Me-P (blacked filled and open triangles), PPA (brown filled and open circles), HEDP (blue filled and open triangles), PIDC (green filled and open circles), HABDP (purple filled and open squares), and ATMP (red filled and open triangles).

dissolution is enhanced at lower solution pH values, with titanium release being highest for the parent mZrTi material in 2 mol/L HNO_3 after 72 h. It follows that functionalized mZrTi variants have a fractional loss below 0.3, with the highest amount preferentially corresponding to MeP-mZrTi at a fractional release of 0.26; PIDC-mZrTi with 0.22; PPA-mZrTi with 0.18; and HEDP, HABDP, and ATMP-mZrTi all within a fractional release below 0.08 at 72 h. An acid dependence can be observed at this point for 24 and 72 h time points. Research on oxide-based materials have shown that dissolution reactions of titanium are initiated by the surface coordination of the material with H^+ and ligands that polarize, weaken, and tend to break the metal−oxygen bonds of the surface.[31] Therefore, durability of titanium oxide in acidic solutions can be envisaged as occurring by a parallel dissolution mechanism involving H^+ and ligands existing in solution. Unlike preferred complexing anions such as SO_4^{2-} or Cl^-, NO_3^- is a much weaker complexing agent, with very dilute HNO_3 known to be nonoxidizing.[32] Cotton et al. suggests oxidation only becomes significant when concentrations of HNO_3 become greater than 2 mol/L.[33] Therefore, the effect of leaching with HNO_3 can be largely attributed to H^+ attack that renders the surface positively charged. Functional group

dx.doi.org/10.1021/am3031695 | ACS Appl. Mater. Interfaces 2013, 5, 4120−4128

coverage also appears to do little to hinder the dissolution of titanium, with all phosphonate groups showing some degree of titanium oxide leaching, indicating that a significant portion of the available surface does not contain any grafted molecules and evidently clarifying that surface space still remains for attachment of unbound molecules.

3.2.3. Zirconium Leaching. The dissolution of zirconium from P-mZrTi and unfunctionalized mZrTi are graphed in Figure 3. The influence of acid concentration on Zr leaching is

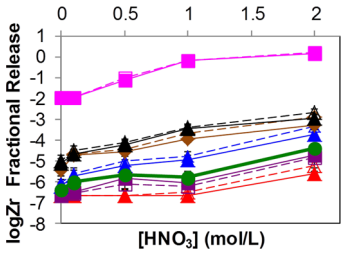

Figure 3. Leaching of Zr from mZrTi and P-mZrTi materials in varying HNO_3 concentrations (2−0.001 mol/L) for 24 and 72 h; mZrTi (pink filled and open squares), Me-P (black filled and open triangles), PPA (brown filled and open circles), HEDP (blue filled and open triangls), PIDC (green filled and open circles), HABDP (purple filled and open squares), and ATMP (red filled and open triangles).

similar to that of Ti, where the parent mZrTi material has the highest fractional release values in 2 mol/L HNO_3 compared to the functionalized variants. However, the fraction of Zr loss is in general an order of magnitude lower than that of Ti. This is most likely due to the inherent stability of Zr−O bonds toward hydrolysis under oxidizing acid conditions. Although the Zr and Ti distribution of the present materials has been observed to be homogeneous on the scale of observation permitted by transmission electron microscopy, this does not exclude the possibility of local regions of (Zr−O−Zr)x bonding. The pronounced durability of zirconium oxide in nitric acid is well-known for nanoparticles and films and can be extended here to zirconium titanate mesoporous materials from the results obtained.[34,35] This is consistent with larger Zr−O bond strength of 776.1 kJ/mol compared with 672.4 and 335 kJ/mol for Ti−O and P−O bonds.[36,37] Moreover, Hoebbel et al. suggest that a low hydrolytic stability of metal oxide complexes without functionality result in an additional, mostly indefinite number of H^+ groups at the metal centers which causes a higher degree of hydrolysis reactions compared to stable complexes with a defined organic functionality.[38]

3.2.4. Leaching Kinetics. With the fractional P release at steady state well below 0.5 for most ligands, only MeP-mZrTi and PIDC-mZrTi were selected for further study of the elemental dissolution kinetics at particular acid concentrations over a 24 h period (Figure 4). The dissolution of P, Ti, and Zr as a function of time in 0.001 and 2 mol/L HNO_3 are displayed in Figure 4a−c. Each data point represents a mean of triplicate measurements for each material. The first noteworthy feature of the kinetic data is that the bare surfaces leach severely compared with the surfaces of the functionalized variants. Indeed, almost complete dissolution of the unfunctionalized mZrTi is observed within 400 min in 2 mol/L HNO_3. A second feature of the data is that although the kinetic plots for P and Ti dissolution show essentially a parabolic process, the case for Zr leaching kinetics appears to be different for the functionalized materials (MeP and PIDC). In the case of Zr, two processes

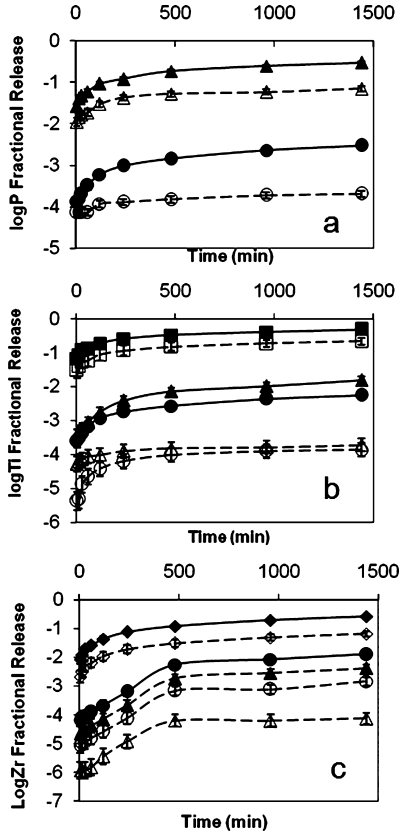

Figure 4. Leaching graphs of (a) P, (b) Ti, and (c) Zr in 0.001 (open points) and 2 (closed points) mol/L HNO_3 concentrations over 24 h. Ti (■, □) and Zr (◇, ◆) release from mZrTi; PIDC (▲, Δ) and Me-P (●, ○) from P-mZrTi.

seem to be operative. The first process is characterized by a rapid initial release rate (fast surface reaction) of these elements below 200 min and the second a parabolic process culminating in what appears to be a steady state up to 1440 min. Release differs however for PIDC-mZrTi and mZrTi at 0.001 mol/L HNO_3 with all elements invariant throughout the experiment, indicating good durability at this particular concentration. This may further emphasize that solution acidity increases elemental dissolution owing to enhanced protonation of surface molecules leading to changes in surface potential of the material. Dissolution profiles acquired at 2 mol/L HNO_3 were found to have statistical significances at all time points ($p < 0.001$) in relation to both control experiments at $t = 0$ and among the materials ($p < 0.05$, where p is the Poisson regression value obtained from the ANOVA analysis. See Experimental Section) with repeated analysis of variance. Analysis of variance was rendered insignificant for all experiments conducted at 0.001 mol/L HNO_3 ($p > 0.05$), showing release to be incomplete and far from equilibrium. To facilitate interpretation of the dissolution data a parabolic dissolution model has been applied as suggested by Stumm[39]

$$Q_i = Q_0 + k_i t^{1/2} \quad (2)$$

This model assumes a diffusion controlled process. In the above expression Q_i is the amount of element released into solution (mg g^{-1}), k_i is the parabolic rate constant (mg g^{-1} $min^{-1/2}$) and Q_0 is the quantity of material (mg g^{-1}) exchanged during initial surface contact with the liquid phase. Plots of element release versus time$^{1/2}$ give straight lines as shown in Figure S5a−c in

dx.doi.org/10.1021/am3031695 | ACS Appl. Mater. Interfaces 2013, 5, 4120−4128

the Supporting Information. The linearity of the data supports dissolution from the mesopores being consistent with diffusion controlled transport processes, with the rate limiting step being the movement of P, Ti, and Zr through a diffusion layer to the solution phase. The parabolic rate constant k can then be extrapolated by applying least-squares regression analysis on the data and are found in Table S4 (see the Supporting Information). For the plots of Figure S4 in the Supporting Information, coefficients greater than 0.90 are consistently observed. The similarity of all the curves suggests a diffusion-controlled process in all cases. In line with qualitative observations of the data in Figure 4, higher rate constants are seen for release of all elements in 2 mol/L HNO_3. The marked difference in rate constants for the three elements suggests that dissolution is incongruent. Clearly, the dissolution of Ti occurs at a much faster rate than for P and Zr. For instance Ti release for each mZrTi, MeP-mZrTi, and PIDC-mZrTi rate constants of 1.44, 1.37, and 1.23 mg g^{-1} $min^{-1/2}$ were observed, respectively. For the release of P from MeP-mZrTi and PIDC-mZrTi values of 1.31 and 1.08 mg g^{-1} $min^{-1/2}$ were observed. Values of Q_0 follow in much the same sequence, indicating greater Ti and P concentrations in the initial solution at a HNO_3 concentration of 2 mol/L as previously suggested on the basis of equilibrium data (compare Figures 3 and 4). Clearly, the lower kinetic constant for Zr dissolution in all cases suggests that Zr−O−P bonds are stronger and more stable to acid attack than Ti−O−P bonds. This hypothesis is supported by recent observations of the enhanced strength of complexation of phosphonates to zirconium oxide surfaces relative to titanium oxide.[16,28]

3.3. DRIFT Spectroscopy after Leaching. To aid in assessing changes in chemical structure and overall monolayer attachment after treatment, we present DRFIT spectra (900−1800 cm^{-1}) of P-mZrTi and mZrTi before and after leaching in 2 mol/L HNO_3 in panels a and b in Figure 5, respectively. Spectra over the range 900 − 3600 cm^{-1} of samples before and after leaching are provided in the Supporting Information section. By comparing the spectra of the as-prepared samples (Figure 5a) to the spectra of the leached samples (Figure 5b) it is clear that changes in the bonding of functional molecules have occurred. As indicated previously in section 3.2, absorption bands in the range 900−1250 cm^{-1} belong to phosphonic acid moieties. For the P═O vibrations around 1200−1130 cm^{-1} a significant decrease in relative intensity is observed. This is especially true for HABDP, HEDP, and PIDC-mZrTi where the broadening and weakening of this band is quite pronounced, indicating either the loss of monolayers to the leaching solution or that leaching has induced the elimination of free phosphonate groups with all phosphoryl oxygen atoms now coordinated to the zirconium titanate surface. The latter, seems most likely as only a small loss of HABDP, HEDP, and PIDC ligands are observed after leaching in 2 M HNO_3 for 24 h. Additionally, a more intense shoulder observed for PPA-mZrTi at 1055 cm^{-1} is also an indication that the PPA ligand may show a greater tendency for tridentate coordination after leaching. Evidence of a band at 1100 cm^{-1} before and after leaching does however imply that PPA still contains P═O groups belonging to free phosphonates. A 2-fold decrease in the intensity of this band in the phosphoryl region for MeP-mZrTi indicates lower surface coordination of the MeP after leaching with the hydration of PO_4^{3-} ions leading to detachment, diffusion across the surface and subsequent release into solution. The fact that a decrease in the peak

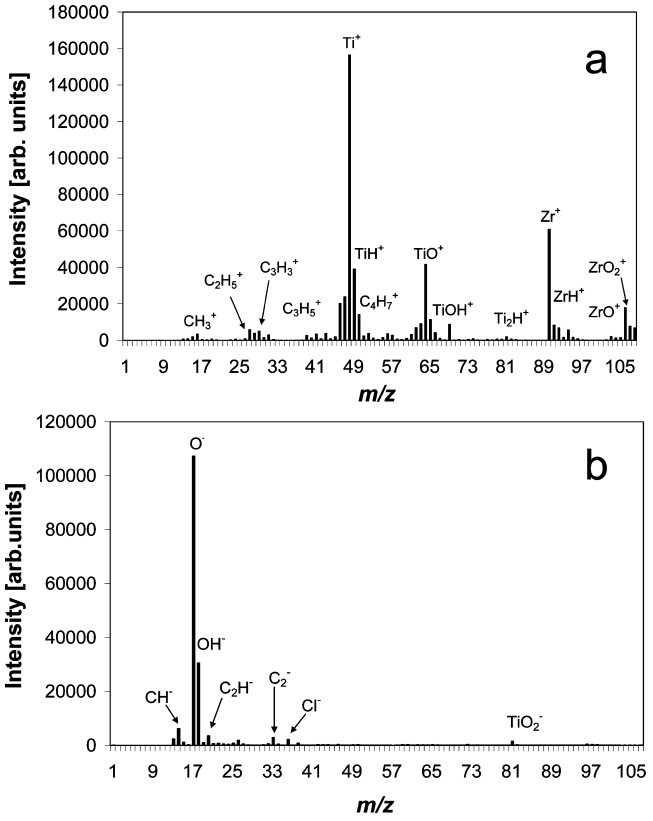

Figure 5. Positive and negative ToF-SIMS spectra obtained for unfunctionalized mZrTi.

intensity is observed for ATMP-mZrTi indicates that the trisphosphonate remains highly stable under the given conditions. A sharp band belonging to an NO_3^- asymmetric stretch in the range 1390−1400 cm^{-1} indicates HNO_3 coordination to the surface after leaching.[40] These absorption bands have been reported previously by Goodman et al. on oxide surfaces who assign them to degenerate ν_3 modes of NO_3^- and NO_2 coordinated in monodentate, bidentate, and bridging fashion, which has been split into two bands because of loss of symmetry upon adsorption.[41]

3.4. ToF-SIMS Analysis after Leaching. Subsequent to leaching in 2 mol/L HNO_3 for 24 h, P-mZrTi and mZrTi were analyzed by ToF-SIMS to probe the surface of any remanent monolayer coverage within the pores. Positive and negative ion ToF-SIMS spectra in the mass range of 0−110 m/z of unfunctionalized mZrTi after 2 mol/L leaching is shown in Figures 6a and b at a mass range of 0- 110 m/z. It clear that the composition of the material belongs to that of the zirconium titanate framework, with an array of characteristic peaks identified in both static spectra. Moreover, it seems the surface has not changed dramatically in terms of its stoichiometry as the intensity of these peaks is quite pronounced. The most intense readings in the positive spectrum originate from fragments of Ti^+ (m/z = 48), its corresponding isotopes and hydrated species TiH^+, TiO^+, $TiOH^+$, and Ti_2H^+ (m/z = 47, 64, 68, 81). Also found are molecular isotopes of Zr^+ (m/z = 90) and related ions ZrH^+, ZrO^+ and ZrO_2^+ (m/z = 91, 106, 108). These findings are in reasonable agreement with the literature and also with the leaching studies in section 3.2 as the intensity of Zr found is almost half that of Ti.[42,43]

A few artifacts belonging to atmospheric hydrocarbons are also present, namely fragmentation of the $C_xH_y^+$ type. The

dx.doi.org/10.1021/am3031695 | ACS Appl. Mater. Interfaces 2013, 5, 4120−4128

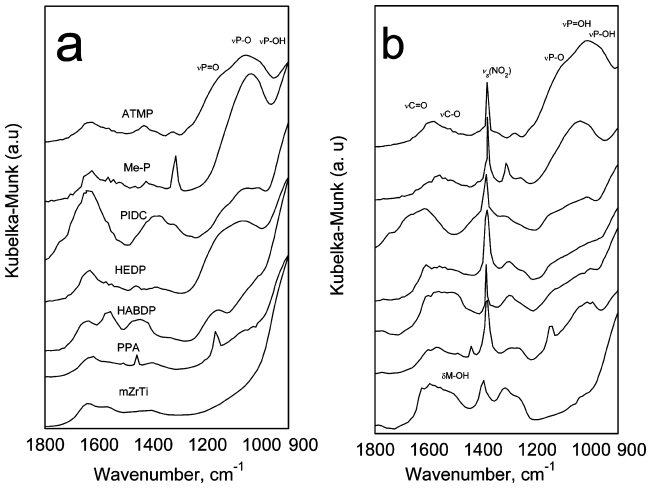

Figure 6. DRIFT spectra of P-mZrTi and mZrTi at 1800−900 cm^{-1} for (a) before and (b) after leaching at 2 M HNO_3 for 24 h.

analogous negative ion spectrum is typical of hydroxylated surfaces inundated by O^- at m/z = 16 and OH^- at m/z = 17 respectively, along with sputtering of TiO_2^- and ZrO_2^- (m/z = 80, 126) at lower intensities. Contamination by $C_xH_y^-$, C_2^- and Cl^- were also present. Small peaks of mixed metal species attributed to $ZrTiO_2$ in the form $Zr_xTi_yO_z^{\pm}$ were also found at higher mass range (i.e., $ZrTiO_3^{\pm}$ and $ZrTiO_4^{\pm}$ at m/z = 191, 202) representative of the Ti−O−Zr network composition consistent with literature.[44] No specific changes occur in the positive spectra of the modified materials in relation to the unmodified spectra, though the intensity of the Ti and Zr peaks had decreased slightly, implying that only a relatively small fraction of the ligand remains and/or that the strength of the acid on the detachment of the surface ligands was effective. This coincides well with findings of Viornery et al. and Adden et al..[43,45] Fragmentation analysis of the remaining phosphonic acid modified materials in the negative spectrum are summarized in Table S4 (see the Supporting Information). New characteristic peaks providing confirmation of phosphonic acid (P^-, PO^-, PO_2^-, PO_3^-, HPO_3^-, and $H_2PO_3^-$) surface attachment is evident in all modified materials; a positive indication of both chemisorbed monolayers and its presence on the surface after acid treatment. Although appearing as smaller peaks above m/z > 100, organometallic fragmentation of the type $Ti_wO_xP_yH_z$, $Zr_wO_xPyH_z$, and $ZrTiO_xP_yH_z$ are also present, confirming that both the oxide layer of the mesoporous material is directly bound to the phosphonic acid groups and demonstrating P−O−Ti, P−O−Zr, and Zr−O−P−O−Ti moieties still remain after contact with the acid solution. Further, individual organic clusters of the form $C_wH_xP_yO_z$ characteristic of each ligand are observed, strongly confirming the incorporation of phosphonic acid groups on the oxide surface. These measurements demonstrate the potential of ToF-SIMS for trace monolayer detection even at very low concentrations, which could not be observed when analyzed with solid state NMR.

3.5. Effect of Leaching on Porosity. To ascertain whether the leaching that has been observed has had a significant impact on the mesostructural texture of the materials, we measured nitrogen adsorption−desorption isotherms of the unfunctionalized parent material and selected functionalized variants (MeP, PIDC and ATMP) before and after leaching. The BET surface areas of the samples together with pore diameters calculated using the BJH method are provided in Table 2. Isotherms and pore size distribution (PSD) plots for mZrTi

Table 2. BET Surface Area and BJH Pore Diameters of Variously Functionalized mZrTi Samples

sample	S_{BET} (m^2/g)	pore diameter (Å)
mZrTi	263.9	23.5
mZrTi leached	291.8	24.0
MeP-mZrTi	197.3	22.5
MeP-leached	228.2	22.3
PIDC-mZrTi	201.1	22.6
PIDC-mZrTi leached	216.7	22.2
ATMP-mZrTi	227.6	22.7
ATMP -mZrTi leached	221.4	22.3

and the most leachable of the functionalized variants (MeP-mZrTi) are provided in Figures 7 and 8. The isotherms of the

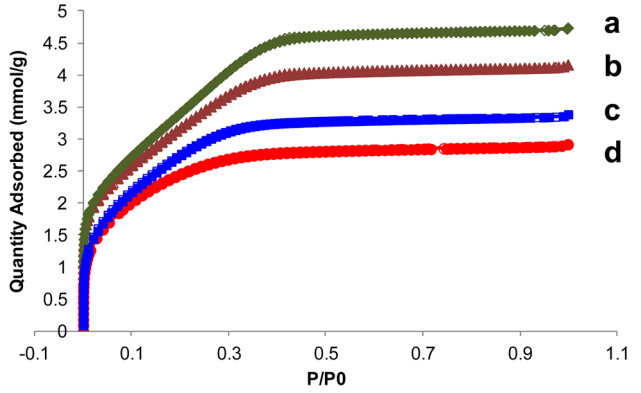

Figure 7. Nitrogen adsorption−desorption isotherms of (a, b) leached and unleached mZrTi and (c, d) leached and unleached MeP-mZrTi (closed and open symbols are the adsorption and desorption branches).

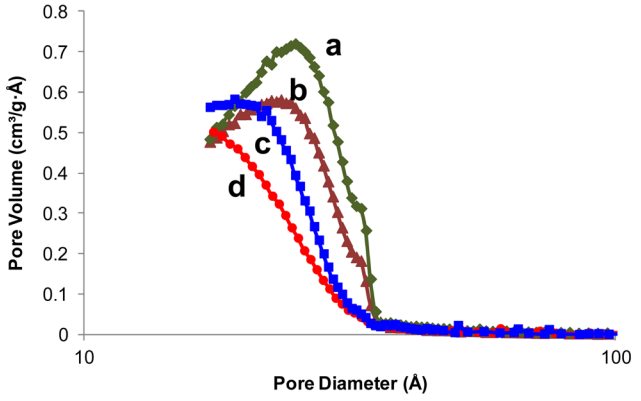

Figure 8. BJH pore size distribution for (a, b) leached and unleached mZrTi and (c, d) leached and unleached MeP-mZrTi.

mZrTi material are consistent with what was previously published.[5] Leaching of this material in 2 M HNO_3 for 24 h did not dramatically alter the overall isotherm shape or the PSD, although it resulted in a 10.5% increase in surface area. For monophosphonate functionalized material (MeP-mZrTi), for which the phosphonate loading was highest, the isotherm was noticeably altered and appeared closer to a Type II isotherm characteristic of microporous materials. Indeed, the

PSD was noticeably shifted to lower pore diameters consistent with the observed reduction in surface area from 264 to 197 m^2/g after MeP funtionalization. Of the hybrids investigated, the monophosphonate functionalized material gave the greatest degree of leaching and the partial restoration of surface area to 227 m^2/g after leaching is consistent with reopening of pore space. For the PIDC-mZrTi and ATMP-mZrTi materials that were leached to a far lesser extent, the isotherms and resultant PSDs were little changed from their original values (see Figures S5 and S6 of the Supporting Information section). These porosity data highlight the fact that the polyphosphonates are hydrolytically resilient, tolerating rather extreme conditions without leaching significantly, or suffering great degradation of the mesoporous texture.

The results show that although the loading of ATMP and the other bisphosphonates is lower than for the monophosphonates (MeP and PPA), the level of surface protection afforded by the polyphosphonates is far greater than for monophosphonates. We hypothesize that this enhanced stability is the result of strong multidentate coordination of the polyphosphonate groups to more reactive regions of the mixed oxide surface.

4. CONCLUSIONS

The successful functionalization of phosphonic acid groups to the surface of zirconium titanium oxide xerogels has been confirmed. The results obtained from thermal analysis suggest functionalization occurs by distinctly different mechanisms, influenced by the mode of coordination to the surface as postulated previously. Depending on the type of phosphonate anchored to the surface, bonding modes can vary between mono-, bi-, and tridentate coordination and are seen to essentially anchor through condensation reactions. These functionalized materials also display different behaviors in acidic solution, with stability based on ligand−metal interactions as well as depending on the concentration/pH conditions of the solution. Furthermore, the stability depends on the size and the number of phosphonic acid groups bound to the surface as the most stable ligands are those that possess two or more phosphonate groups. Dissolution of Ti, Zr, and P could be described by concentration-dependent kinetics, with the release being greatest for unmodified mZrTi and bound methylphosphonic acid (MeP). Through ToF-SIMS and FT-IR chemisorbed phosphonates are still evident following leaching in strong acid. Because the dissolution rate of Zr is much lower than that of P and Ti, it is hypothesized that the stronger Zr−O−P bond and the stronger binding of phosphonate groups to Zr surface sites are responsible for this incongruent dissolution. This suggests that in applications where acid stability is critical, zirconium rich compositions are favored. Polyphosphonate functionalized materials are extremely stable even in 2 M HNO_3 suggesting that they can be contemplated for use in relatively harsh environments. For radioactive waste management applications, they would, however, also have to display good radiolytic stability. This will be the subject of a future contribution.

■ ASSOCIATED CONTENT

Supporting Information

Thermogravimetric analysis traces, solid-state P-31 MAS NMR, FTIR data, kinetic analyses, and nitrogen adsorption−desorption isotherms for the variously functionalized mZrTi samples. This material is available free of charge via the Internet at http://pubs.acs.org.

■ AUTHOR INFORMATION

Corresponding Author

*E-mail: vluca@cnea.gov.ar. Tel.: 54-11-6772 7018.

Notes

The authors declare no competing financial interest.

■ ACKNOWLEDGMENTS

The authors acknowledge Dr. John Denman of the Ian Wark Institute, University of South Australia for measurements of ToF-SIMs spectra and Dr. Eric. R Vance and Dr. Tracey L. Hanley for useful discussions. M.D. is supported by the Australian Research Council Nanotechnology Network (ARCNN) Long-Term Visitor Fellowship.

■ REFERENCES

(1) Hoffmann, F.; Cornelius, M.; Morell, J.; Froba, M. *Angew. Chem., Int. Ed.* **2006**, *45*, 3216.
(2) Fryxell, G. E.; Lin, Y. H.; Fiskum, S.; Birnbaum, J. C.; Wu, H.; Kemner, K.; Kelly, S. *Environ. Sci. Technol.* **2005**, *39*, 1324.
(3) Lebed, P. J.; de Souza, K.; Bilodeau, F.; Larivie, D.; Kleitz, F. *Chem. Commun.* **2011**, *47*, 11525.
(4) Zuo, L.; Tian, X.; Yu, S.; Jiang, J.; Zhou, H. *J. Radioanal. Nucl. Chem.* **2011**, *288*, 378.
(5) Luca, V.; Bertram, W.; Widjaja, J.; Mitchell, D. R. G.; Griffith, C. S.; Drabarek, E. *Microporous Mesoporous Mater.* **2007**, *103*, 123.
(6) Strachan, D. M.; Scheele, R. D.; Buck, E. C.; Kozelisky, A. E.; Sell, R. L.; Elovich, R. J.; Buchmiller, W. C. *J. Nucl. Mater.* **2008**, *372*, 16.
(7) Lumpkin, G. R. *Elements* **2006**, *2*, 365.
(8) Omel'yanenko, B. I.; Livshits, T. S.; Yudintsev, S. V.; Nikonov, B. S. *Geol. Ore Deposits* **2007**, *49*, 173.
(9) Griffith, C. S.; Sizgek, G. D.; Sizgek, E.; Scales, N.; Yee, P. J.; Luca, V. *Langmuir* **2008**, *24*, 12312.
(10) Mutin, P. H.; Lafond, V.; Popa, A. F.; Granier, M.; Markey, L.; Dereux, A. *Chem. Mater.* **2004**, *16*, 5670.
(11) Mutin, P. H.; Guerroro, G.; Vioux, A. *C. R. Chim.* **2003**, *6*, 1153.
(12) Mutin, P. H.; Guerrero, G.; Vioux, A. *J. Mater. Chem.* **2005**, *15*, 3761.
(13) Guerrero, G.; Mutin, P. H.; Vioux, A. *Chem. Mater.* **2001**, *13*, 4367.
(14) Angelome, P. C.; Soler-Illia, Gjdaa *Chem. Mater.* **2005**, *17*, 322.
(15) Queffélec, C.; Petit, M.; Janvier, P.; Knight, D. A.; Bujoli, B. *Chem. Rev.* **2012**, *112*, 3777.
(16) Griffith, C. S.; Reyes, M. D. L.; Scales, N.; Hanna, J. V.; Luca, V. *ACS Appl. Mater. Interfaces* **2010**, *2*, 3436.
(17) Sizgek, G. D.; Sizgek, E.; Griffith, C. S.; Luca, V. *Langmuir* **2008**, *24*, 12323.
(18) Makowski, P.; Deschanels, X.; Grandjean, A.; Meyer, D.; Toquerand, G.; Goettmann, F. *New J. Chem.* **2012**, *36*, 531.
(19) Luechinger, M.; Prins, R.; Pirngruber, G. D. *Microporous Mesoporous Mater.* **2005**, *85*, 111.
(20) Etienne, M.; Walcarius, A. *Talanta* **2003**, *59*, 1173.
(21) Gopi, D.; Manimozhi, S. G. K. M.; Manisankar, P.; Rajeswari, S. *J. Appl. Electrochem.* **2007**, *37*, 439.
(22) Pellerite, M. J.; Dunbar, T. D.; Boardman, L. D.; Wood, E. J. *J. Phys. Chem. B.* **2003**, *107*, 11726.
(23) Badia, A.; Lennox, R. B.; Reven, L. *Acc. Chem. Res.* **2000**, *33*, 475.
(24) Bortun, A. I.; Garcķa, J.; Budovitskaya, T. A.; Strelko, V. V.; Rodrķguez, J. *Mater. Res. Bull.* **1996**, *31*, 487.
(25) Marcinko, S.; Fadeev, A. Y. *Langmuir* **2004**, *20*, 2270.
(26) Soler-Illia, G. J. A. A.; Louis, A.; Sanchez, C. *Chem. Mater.* **2002**, *14*, 750.
(27) Parida, K. M.; Mallick, S.; Sahoo, P. C.; Rana, S. K. *Appl. Catal. A. Gen.* **2010**, *381*, 226.
(28) Pawsey, S.; Yach, K.; Reven, L. *Langmuir* **2002**, *18*, 5205.
(29) Bae, E.; Choi, W.; Park, J.; Shin, H. S.; Kim, S. B.; Lee, J. S. *J. Phys. Chem. B* **2004**, *108*, 14093.

(30) Lecollinet, G.; Delorme, N.; Edely, M.; Gibaud, A.; Bardeau, J.-F.; Hindr, F.; Boury, F.; Portet, D. *Langmuir* **2009**, *25*, 7828.
(31) Blackwood, D. J.; Chooi, S. K. M. *Corros. Sci.* **2002**, *44*, 395.
(32) Housecroft, C. E. ; Sharpe, A. G. *Inorganic Chemistry*; Prentice Hall: Upper Saddle River, NJ, 2005.
(33) Cotton, F. A.; Murillo, C. A.; Bochmann, M.; Grimes, R. N. *Advanced Inorganic Chemistry*, 6th ed.; Wiley−Interscience, 1999.
(34) Gao, W.; Dickinson, L.; Grozinger, C.; Morin, F. G.; Reven, L. *Langmuir* **1996**, *12*, 6429.
(35) Andreeva, V. V.; Glukhova, A. I. *J. Appl. Chem.* **1961**, *11*, 390.
(36) Kappes, M. M.; Staley, R. H. *J. Phys. Chem.* **1981**, *85*, 942.
(37) Van Noort, R.; Noroozi, S.; Howard, I. C.; Cardew, G. *J. Dentistry* **1989**, *17*, 61.
(38) Hoebbel, D.; Reinert, T.; Schmidt, H.; Arpac, E. *J. Sol−Gel Sci. Technol.* **1997**, *10*, 115.
(39) Stumm, W. *Aquatic Surface Chemistry: Chemical Processes at the Particle−-Water Interface*; John Wiley: New York, 1987.
(40) Baltrusaitis, J.; Schuttlefield, J.; Jensen, J. H.; Grassian, V. H. *Phys. Chem. Chem. Phys.* **2007**, *9*, 4970.
(41) Goodman, A. L.; Bernard, E. T.; Grassian, V. H. *J. Phys. Chem. A.* **2001**, *105*, 6443.
(42) Zhang, B. S.; Barth, G.; Liu, H. K.; Chang, S. *Appl. Surf. Sci.* **2004**, *231−232*, 868.
(43) Viornery, C.; Chevolot, Y.; Léonard, D.; Aronsson, B.; Péchy, P.; Mathieu, H. J.; Descouts, P.; Grätzel, M. *Langmuir* **2002**, *18*, 2582.
(44) Ruppert, A.; Paryjczak, T. *Russ. J. Phys. Chem.* **2005**, *79*, 1054.
(45) Adden, N.; Gamble, L. J.; Castner, D. G.; Hoffmann, A.; Gross, G.; Menzel, H. *Langmuir* **2006**, *22*, 8197.